ELSEVIER

Journal of Organometallic Chemistry 626 (2001) 118–124

Journal of Organometallic Chemistry

www.elsevier.nl/locate/jorganchem

Novel complexes *cis*,*cis*-[Rh(R)$_2$(I)(CO)(dmb)] (R = Me, ^{i}Pr; dmb = 4,4′-dimethyl-2,2′-bipyridine): synthesis, structure and photoreactivity

Joris van Slageren [a], Anne Louise Vermeer [a], Derk J. Stufkens [a,*], Martin Lutz [b], Anthony L. Spek [b]

[a] *Institute of Molecular Chemistry, Universiteit van Amsterdam, Nieuwe Achtergracht 166, NL-1018 WV Amsterdam, The Netherlands*
[b] *Bijvoet Center for Biomolecular Research, Department of Crystal and Structural Chemistry, Utrecht University, Padualaan 8, NL-3584 CH Utrecht, The Netherlands*

Received 2 October 2000; received in revised form 3 January 2001; accepted 3 January 2001

Abstract

The synthesis, structure and photochemistry of the novel rhodium(III) complexes *cis*,*cis*-[Rh(R)$_2$(I)(CO)(dmb)] (R = Me (**1**), ^{i}Pr (**2**)) are reported. Although many di- and trimethyl–rhodium(III) complexes are known, *cis*,*cis*-[Rh(^{i}Pr)$_2$(I)(CO)(dmb)] (**2**) is the first diisopropyl–rhodium(III) compound. Single-crystal X-ray diffraction studies revealed the structure of **1**. Resonance Raman spectra were obtained by excitation into the lowest-energy allowed electronic transition of the complexes. These spectra show that this transition has halide-to-ligand charge transfer (XLCT) character. Upon irradiation in solution, both **1** and **2** give rise to Rh–R bond homolysis as evidenced by IR, UV–vis and spin-trap EPR investigations. The photoreaction is proposed to occur after crossing from the XLCT state to the reactive sigma-bond-to-ligand charge transfer (SBLCT) state. For the ^{i}Pr-complex homolysis is observed at longer wavelength irradiation than for the methyl derivative, indicating that in the former case the reactive state is lower in energy.

Keywords: Rhodium–alkyl complexes; Crystal structures; Resonance Raman spectra; Photochemistry; EPR spectra

1. Introduction

Complexes with a lowest metal-to-ligand charge transfer (MLCT) state, such as [Ru(bpy)$_3$]$^{2+}$ and [Re(Cl)(CO)$_3$(bpy)] have been extensively studied with regard to their excited state properties. If the chloride in the latter complex is replaced by a strongly σ donating ligand L, such as an alkyl group or metal fragment, σ(Re–L) of [Re(L)(CO)$_3$(α-diimine)] may become the HOMO, and the lowest excited state obtains σ(Re–L)→(α-diimine) or sigma-bond-to-ligand charge transfer (SBLCT) character [1,2]. The photochemical properties of such complexes [Re(L)(CO)$_3$(α-diimine)] have been studied extensively in our laboratory [3–5]. These studies showed that occupation of the SBLCT excited state can give rise to efficient Re–L bond homolysis. More recently, these studies were extended to [M(L$_1$)(L$_2$)(CO)$_2$(α-diimine)] (M = Ru, Os) and [Pt(L)$_2$(Me)$_2$(α-diimine)] [6–8]. However, only a few

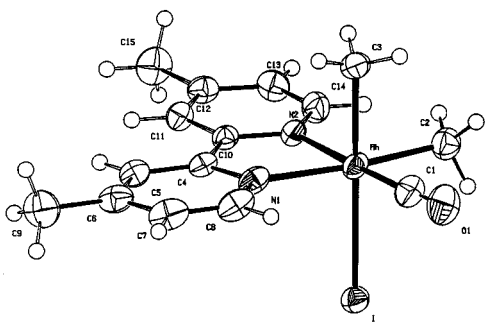

Fig. 1. Displacement ellipsoid plot of **1** (50% probability level). The CH_2Cl_2 molecule, present in the asymmetric unit, has been omitted for clarity. The methyl and carbonyl groups in the equatorial plane are disordered: The ligand position at C1 consists of 67.7(7)% carbonyl and 32.3(7)% methyl; the ligand position at C2 vice versa.

* Corresponding author. Tel.: +31-20-5256451; fax: +31-20-5256456.
E-mail address: stufkens@anorg.chem.uva.nl (D.J. Stufkens).

0022-328X/01/$ - see front matter
PII: S0022-328X(01)00676-3

complexes are known that contain a Group 9 transition metal atom, having low lying SBLCT states. One well studied example is vitamin B12 and its model complexes [9], for which the SBLCT excited state was proposed to be responsible for the observed Co–C bond splitting [10]. Apart from these examples, to our knowledge the only Group 9 organometallic complexes shown to possess such SBLCT excited states are *fac*-[Ir(III){tris - (6 - isopropyl - 8 - quinolyl)diorganosilyl}] [11,12], and $[Ir(R)(CO)(PPh_3)_2(mnt)]$ (R = Me, Et; mnt = maleonitriledithiolate) [13].

As an extension of our photochemical investigations of d^6 transition metal–alkyl complexes, such as $[Re(R)(CO)_3(\alpha\text{-diimine})]$ (R = Me, Et, Bzl) [4,14], and $[Ru(I)(R)(CO)_2(\alpha\text{-diimine})]$ (R = ^{i}Pr, Bzl) [15,16], we present here the synthesis, structure and photochemistry of two novel complexes *cis*,*cis*-$[Rh(R)_2(I)(CO)(dmb)]$ (R = Me (**1**), ^{i}Pr (**2**); dmb = 4,4′-dimethyl-2,2′-bipyridine), with the iodide ligand in an axial position (Fig. 1). They are in fact, to our knowledge, the first Rh-complexes containing both alkyl and α-diimine ligands. This combination of ligands may lead to radical formation upon visible-light excitation.

2. Experimental

2.1. Materials

I_2 (Merck), 4,4′-dimethyl-2,2′-bipyridine (dmb, Fluka), MeMgCl (3.0 M in THF, Aldrich), ^{i}PrMgCl (2.0 M in THF, Aldrich), $AgNO_3$ (Aldrich, 99%) were used as received. Solvents purchased from Acros (THF, hexane, pentane, dichloromethane, methanol) were dried on and distilled from the appropriate drying agent. Silica gel (kieselgel 60, Merck, 70–230 mesh) for column chromatography was dried and activated by heating in vacuo at 160°C overnight.

2.2. Syntheses

All syntheses were performed under a nitrogen atmosphere using standard Schlenk techniques. $[Rh(Cl)(CO)_2]_2$ was prepared according to a literature procedure [17].

2.2.1. [Rh(Cl)(CO)(dmb)]

To a solution of $[Rh(Cl)(CO)_2]_2$ in THF, 1.1 equivalents of dmb in THF was added at −78°C. The reaction mixture was allowed to warm to room temperature (r.t.) while stirring. Evaporation of the solvent and washing with hexane afforded the red product as a solid in ca. 90% yield. IR (THF); ν(CO): 1970 cm^{-1}. UV (THF); λ_{max}: 501 nm. ^{1}H-NMR ($CDCl_3$); δ: 2.42 (s, 6H, dmb CH_3), 2.54, (s, 6H, dmb CH_3), 7.04 (d, $^3J = 5.6$ Hz, 2H, dmb H5), 7.29 (d, $^3J = 5.9$ Hz, 2H, dmb H5), 7.76 (s, 1H, dmb H3), 7.80 (s, 1H, dmb H3), 8.51 (d, $^3J = 5.6$ Hz, 2H, dmb H6), 9.16 (d, $^3J = 5.8$ Hz, 2H, dmb H6) ppm.

2.2.2. [Rh(NO$_3$)(CO)(dmb)]

A suspension of exactly one equivalent of $AgNO_3$ in a solution of 150 mg [Rh(Cl)(CO)(dmb)] in THF was stirred overnight at r.t. Filtration and evaporation of the solvent gave the red product in near quantitative yield. IR (THF); ν(CO): 1970 cm^{-1}. ^{1}H-NMR ($CDCl_3$); δ: 2.42 (6H, dmb CH_3), 2.54, (6H, dmb CH_3), 7.04 (2H, dmb H5), 7.29 (2H, dmb H5), 7.76 (1H, dmb H3), 7.80 (1H, dmb H3), 8.51 (2H, dmb H6), 9.16 (2H, dmb H6) ppm.

2.2.3. [Rh(I)$_2$(NO$_3$)(CO)(dmb)]

Dropwise addition of one equivalent of I_2 in THF to a suspension of 100 mg of $[Rh(NO_3)(CO)(dmb)]$ in THF at −78°C, overnight stirring at r.t. and subsequent evaporation of the solvent yielded the crude product. Washing with pentane gave the pure orange-brown product in ca. 80% yield. IR (THF); ν(CO): 2098 cm^{-1}. ^{1}H-NMR ($CDCl_3$); δ: 2.64 (s, 6H, dmb CH_3), 2.68 (s, 6H, dmb CH_3), 7.35 (d, $^3J = 5.8$ Hz, 2H, dmb H5), 7.55 (d, $^3J = 6.3$ Hz, 2H, dmb H5), 7.99 (s, 2H, dmb H3), 8.66 (d, $^3J = 6.0$ Hz, 2H, dmb H6), 9.69 (d, $^3J = 5.9$ Hz, 2H, dmb H6) ppm.

2.2.4. *cis*,*cis*-[Rh(Me)$_2$(I)(CO)(dmb)] (**1**)

To a solution of $[Rh(I)_2(NO_3)(CO)(dmb)]$ (100 mg) in THF at −78°C, two equivalents of MeMgCl (3.0 M in THF) were gradually added through a syringe, while following the reaction by IR. The colour of the reaction mixture changed from brown to brown–red during the addition. The solid obtained after quenching of the excess of Grignard with MeOH and evaporation of the solvent in vacuo, was dissolved in CH_2Cl_2 and washed repeatedly with water. Drying on anhydrous $MgSO_4$ and evaporation of the solvent yielded the crude product which was purified by column chromatography (activated silica, CH_2Cl_2/hexane gradient elution) and obtained as a yellow-brown solid in ca. 50% yield. FAB-MS; m/z: [M^+] not detected, 817 [$2M^+$–I] (resulting from gas phase clustering), 787 [$2M^+$–I–2 Me], 457 [M^+–Me], 345 [M^+–I], 315 [M^+–2Me–I], 287 [M^+–2Me–I–CO]. IR (THF); ν(CO): 2031 cm^{-1}. UV (THF); λ_{max}: 295, 370 nm. ^{1}H-NMR (CD_2Cl_2); δ: 0.54 (d, $J_{Rh-H} = 2.2$ Hz, 3H, Rh–Me_{ax}, assignment corresponding to [18]), 1.18 (d, $J_{Rh-H} = 2.0$ Hz, 3H, Rh–Me_{eq}), 2.53, (s, 3H, dmb CH_3), 7.33 (d, $^3J = 5.6$ Hz, 2H, dmb H5), 7.42 (d, $^3J = 5.3$ Hz, 2H, dmb H5), 8.07 (s, 2H, dmb H3), 8.76 (d, $^3J = 5.6$ Hz, 2H, dmb H6), 8.77 (d, $^3J = 5.3$ Hz, 2H, dmb H6) ppm. ^{13}C-NMR APT (CD_2Cl_2): δ: −0.9 (d, $J_{Rh-C} = 22$ Hz, Rh–Me_{ax}), 6.6 (d, $J_{Rh-C} = 22$ Hz, Rh–Me_{eq}), 21.4 (dmb Me), 123.7

(dmb C3), 123.9 (dmb C3), 127.3 (dmb C5), 127.7 (dmb C5), 147.7 (dmb C6), 151.4 (dmb C6), 150.6 (dmb C4), 151.5 (dmb C4), 152.7 (dmb C2), 155.2 (dmb C2), 191.3 ($J_{Rh-C} = 68$ Hz, CO) ppm.

2.3. *cis,cis-[Rh(^{i}Pr)$_2$(I)(CO)(dmb)]* (**2**)

This complex was synthesized by reaction of [Rh(I)$_2$(NO$_3$)(CO)(dmb)] (100 mg) and two equivalents of ^{i}PrMgCl in THF using the same method as applied for [Rh(Me)$_2$(NO$_3$)(CO)(dmb)]. The reaction product was purified by pentane extraction of the solid obtained after quenching and evaporation of the solvent. The orange–brown product was obtained in 80% yield. FAB-MS; m/z: [M$^+$] not detected, 929 [2M$^+$–I] (resulting from gas phase clustering), 843 [2M$^+$–I–2^{i}Pr], 729 [2M$^+$–I–4^{i}Pr–CO], 701 [2M$^+$–I–4^{i}Pr–2 CO], 401 [M$^+$–I], 315 [M$^+$–2Me–I], 287 [M$^+$–2Me–I–CO]. IR (THF); ν(CO): 2021 cm^{-1}. UV (THF); λ_{max}: 295, 370 nm. ^{1}H-NMR (CD_2Cl_2); δ: 0.72 (pst, $^3J \approx J_{Rh-H} \approx 6.3$ Hz, 3M, Rh–CH(CH_3)$_2$), 0.92 (m, 1H, Rh–CH(CH$_3$)$_2$ (ax, assignment corresponding to [18])), 1.09 (pst, $^3J \approx J_{Rh-H} \approx 6.3$ Hz, 3H, Rh–CH(CH_3)$_2$), 1.24 (m, 3H, Rh–CH(CH_3)$_2$, 1.7 (m, 3H, Rh–CH(CH_3)$_2$), 2.09 (m, 1H, Rh–CH(CH$_3$)$_2$ (eq)), 2.52 (s, 3H, dmb CH$_3$), 2.58 (s, 3H, dmb CH$_3$), 7.36 (d, $^3J = 5.4$ Hz, 1H, dmb H5), 7.43 (d, $^3J = 5.1$ Hz, 1H, dmb H5), 8.02 (s, 2H, dmb H3), 8.61 (d, $^3J = 6.0$ Hz, 2H, dmb H6), 8.76 (d, $^3J = 5.4$ Hz, 2H, dmb H6) ppm. ^{13}C-NMR APT (CD_2Cl_2): δ: 16.9 (d, $J_{Rh-C} = 2.8$ Hz, Rh–CH(CH_3)$_2$), 18.8 (d, $J_{Rh-C} = 2.6$ Hz, Rh–CH(CH_3)$_2$), 21.5 (dmb Me), 27.3 (Rh–CH(CH_3)$_2$), 30.4 (Rh–CH(CH_3)$_2$), 31.7 ($J_{Rh-C} = 22$ Hz, Rh–CH(CH$_3$)$_2$), 33.7 ($J_{Rh-C} = 23$ Hz, Rh–CH(CH$_3$)$_2$), 123.6 (dmb C3), 123.9 (dmb C3), 127.2 (dmb C5), 127.5 (dmb C5), 147.2 (dmb C6), 150.4 (dmb C4), 151.0 (dmb C6), 151.5 (dmb C4), 152.6 (dmb C2), 155.5 (dmb C2), 193.1 ($J_{Rh-C} = 73$ Hz, CO) ppm.

2.4. Measurements

FAB$^+$-MS spectra were obtained on a JEOL JMS SX/SX102A four-sector mass spectrometer coupled to a JEOL MS-MP7000 data system. Infrared spectra were recorded on Bio-Rad FTS-7 and FTS-60A FTIR spectrophotometers (the latter equipped with a liquid-nitrogen-cooled MCT detector), and electronic absorption spectra on Varian Cary 4E and Hewlett–Packard 8453 spectrophotometers. NMR spectra were recorded on a Varian Mercury 300 (300.13 MHz and 75.46 MHz for ^{1}H and ^{13}C, respectively) spectrometer. Resonance Raman spectra of the complexes dispersed in KNO$_3$ pellets were recorded on a Dilor XY spectrometer equipped with a Wright Instruments CCD detector, using a Spectra Physics SP2040E Ar$^+$ laser as the excitation source. EPR spectra were recorded using a Varian E-104A instrument. The radicals were generated by in situ irradiation using an Oriel high pressure mercury lamp. The photochemical reactions were also studied by in situ irradiation of solutions of the complexes inside Varian Cary 4E (UV/Vis) or Bio-Rad FTS-60A (IR) spectrometers with a Spectra Physics SP2025 Ar$^+$ laser.

2.5. Single-crystal structure determination of **1**

Suitable crystals of **1** were grown by vapour diffusion of hexane into a solution of **1** in CH_2Cl_2 at -20°C. Crystal data: $C_{15}H_{18}IN_2ORh{\cdot}CH_2Cl_2$, FW = 557.05, colourless block, $0.36 \times 0.27 \times 0.12$ mm^3, monoclinic, $P2_1/c$ (no. 14), $a = 11.0746(3)$, $b = 14.1766(4)$, $c = 14.5336(4)$ Å, $\beta = 119.462(2)$°, $V = 1986.70(10)$ Å^3, $Z = 4$, $\rho = 1.862$ g cm^{-1}. Intensities were measured on a Nonius KappaCCD diffractometer, with rotating anode (Mo-K$_\alpha$, $\lambda = 0.71073$Å) at 150 K. The absorption correction was based on multiple measured reflections (PLATON [19], $\mu = 2.69$ mm^{-1}, 0.63–0.71 transmission). 17 229 measured reflections, 4538 unique reflections ($R_{int} = 0.0553$). The structure was solved with direct methods (SIR-97 [20]) and refined with the program SHELXL-97 [21] against F^2 of all reflections up to a resolution of $(\sin\theta/\lambda)_{max} = 0.65$ Å^{-1}. The two equatorial ligand positions are partially occupied by methyl and carbonyl groups, respectively. The carbon atoms were not split and refined with an occupancy of 1. For the carbonyl oxygen and the methyl hydrogens the occupancy was refined under the assumption that the total occupancy is 1. The refinement resulted in a disorder ratio of 0.677(7):0.323(7). Non hydrogen atoms were refined freely with anisotropic displacement parameters. Hydrogen atoms were refined as rigid groups. 221 parameters. The drawing, calculations and checking for higher symmetry were performed with the PLATON [19] package. $R(I > 2\sigma(I))$: $R_1 = 0.0275$, $wR_2 = 0.0635$. R(all data): $R_1 = 0.0332$, $wR_2 = 0.0654$. $S = 1.102$.

3. Results and discussion

3.1. Syntheses

The synthesis of [Rh(Cl)(CO)(α-diimine)] from [Rh(Cl)(CO)$_2$]$_2$ was shown in literature to proceed by coordination of the α-diimine resulting in [Rh(Cl)(CO)$_2$(α-diimine)], prior to CO loss [22]. This pentacoordinated complex may dissociate into an [Rh(CO)$_2$(α-diimine)]$^+$(Cl)$^-$ ion pair [23]. Both intermediates were isolated in several cases [24–26]. In contrast, the synthesis of [Rh(Cl)(CO)(dmb)] (dmb = 4,4′-dimethyl-2,2′-bipyridine) did not yield such species in our case. Thus, the product obtained was red in accordance with the observed colour for [Rh(Cl)(CO)(bpy)] [27], whereas e.g. [Rh(CO)$_2$(phen)]$^+$

Table 1
Vibrational data for complexes **1** and **2**

Compound	IR [a] ν(CO) [b]	Resonance Raman [c] (cm^{-1})
$[Rh(Me)_2(I)(CO)(dmb)]$ (**1**)	2031	1621, 1560, 1492, 1322, 1284, 1030, 564, 526
$[Rh(^iPr)_2(I)(CO)(dmb)]$ (**2**)	2021	1621, 1560, 1492, 1326, 1276, 1033, 570, 523, 234
dmb	–	1606, 1561, 1486, 1315, 1290, 1034, 236 [d]

[a] In THF at room temperature.
[b] In cm^{-1}.
[c] In KNO_3.
[d] Selected Raman bands observed on 514.5 nm excitation of the ligand dispersed in a KNO_3 pellet.

Table 2
Important bond lengths (Å) and angles (°) of non-hydrogen atoms of **1** [a]

Bond	Length (Å)	Bonds	Angle (°)
Rh–I	2.7936(3)	I–Rh–N1	89.85(7)
Rh–C1	1.933(5) [b]	I–Rh–N2	90.93(7)
Rh–C2	2.014(3) [b]	I–Rh–C1	92.21(11) [b]
Rh–C3	2.102(3)	I–Rh–C2	92.85(10) [b]
Rh–N1	2.144(3)	I–Rh–C3	179.56(10)
Rh–N2	2.124(2)	N1–Rh–C1	101.55(12) [b]
		C1–Rh–C2	84.93(14) [b]
Dmb	Torsion angle (°)	N2–Rh–C2	96.61(11) [b]
N1–C4–C10–N2	1.0(4)	N1–Rh–N2	76.76(9)

[a] Estimated S.D. values are in parentheses.
[b] Average values, due to methyl/carbonyl disorder (see Section 2).

$(ClO_4)^-$ was reported to be green [25]. Moreover, only one band due to ν(CO) was found in the IR spectrum at 1970 cm^{-1} in THF, in correspondence with literature data for [Rh(Cl)(CO)(bpy)] (1977 cm^{-1} in MeCN) [28]. In addition, ^{1}H-NMR showed the dmb ligand to be in an asymmetric environment, which is not the case for $[Rh(CO)_2(\alpha\text{-diimine})]^+(Cl)^-$.

Apart from these products, the reaction of $[Rh(Cl)(CO)_2]_2$ with an α-diimine ligand afforded $[Rh(CO)_2(Cl)_2]^-$ $[Rh(CO)_2(\alpha\text{-diimine})]^+$ ion pairs [25,26], especially when an excess of $[Rh(Cl)(CO)_2]_2$ was used. Our synthetic procedure did not produce such species.

When [Rh(Cl)(CO)(dmb)] was allowed to react with one equivalent of I_2, a mixture of two products was formed, both of which contain the dmb ligand in an asymmetric environment according to ^{1}H-NMR. Since removal of the chloride ligand, using $AgNO_3$, prior to oxidative addition of I_2, was found to result in a single, pure product, ($[Rh(I)_2(NO_3)(CO)(dmb)]$), the products of the reaction of [Rh(Cl)(CO)(dmb)] with I_2 were not investigated further. NMR showed that the two pyridyl rings of the dmb ligand of $[Rh(I)_2(NO_3)(CO)(dmb)]$ are unequal.

Gradual addition of MeMgCl to $[Rh(I)_2(NO_3)(CO)(dmb)]$ caused the disappearance of the IR band due to the starting compound (2098 cm^{-1}). Initially a band at 2058 cm^{-1} appeared which was in turn replaced by one at 2031 cm^{-1}, indicating successive addition of two methyl groups, to yield $[Rh(Me)_2(I)(CO)(dmb)]$ (**1**). Single-crystal X-ray diffraction studies (vide infra) revealed the structure of **1** to be as depicted in Fig. 1.

Addition of ^{i}PrMgCl to $[Rh(I)_2(NO_3)(CO)(dmb)]$ gave the corresponding orange–brown diisopropyl–rhodium species $[Rh(^iPr)_2(I)(CO)(dmb)]$ (**2**). The ν(CO) vibration has shifted to lower wavenumbers (2021 cm^{-1}), with respect to that of **1** in line with the higher σ-donor strength of the isopropyl group. Although Rh–^{i}Pr complexes are known [29–32], **2** is to our knowledge the first diisopropyl–rhodium complex. Table 1 presents vibrational (IR, resonance Raman) data for complexes **1** and **2**.

3.2. Crystal structure of cis,cis-[Rh(Me)$_2$(I)(CO)(dmb)] (1)

Table 2 lists the most important bond lengths and angles of **1**, while Fig. 1 shows the molecular structure. The coordination environment of the Rh centre is distorted octahedral. The equatorial positions are occupied by the dmb ligand, a methyl and a carbonyl group, while an iodide and methyl group are in the axial ones. The dmb ligand is essentially planar with N–Rh bond lengths of 2.124(2) and 2.144(3) Å. The N–Rh–N angle of 76.76(9)° is significantly smaller than the perfect octahedral angle of 90°. The Rh–I bond length (2.7936(3) Å) is similar to that in $[Rh(Cl)(I)(CH_2I)(CO)(PEt_3)_2]$ (2.803(1) Å) [33], and also to that of the isoelectronic complexes *trans*, *cis*-$[Ru(I)(CH_3)(CO)_2(^iPr\text{–}DAB)]$ (2.7998(9) Å) [34], but slightly shorter than that of $[Pd(I)(Me)_3(bpy)]$ (2.834(1) Å) [35]. The axial Rh–CH_3 bond (2.102(3) Å) is significantly longer than the equatorial one (2.014(3) Å), indicating that the axial Rh–CH_3 bond is weaker (for the methyl carbonyl disorder, see Section 2). A similar situation was encountered for $[Pt(Me)_4(cHx\text{–}DAB)]$ where the axial and equatorial Pt–C bond lengths are 2.140(8) Å and 2.045(5) Å, respectively [18]. In contrast, for $[Pd(I)(Me)_3(bpy)]$, the axial and equatorial Pd–C bond lengths are similar (2.040(6) and 2.034(7)/2.046(7) Å, respectively) [35].

3.3. Electronic absorption and resonance Raman (rR) spectra

Fig. 2 depicts the absorption spectra of **1** and **2** in THF. The spectra of both complexes show the dmb intraligand band at 295 nm as well as an absorption band at ca. 370 nm. Its position is independent of the

nature of the alkyl ligand. The negative solvatochromism ($\Delta\nu = \nu(\text{MeCN}) - \nu(\text{toluene}) \approx 2.2 \times 10^3$ cm^{-1}) shows that the transition belonging to the lowest-energy absorption band has strong charge transfer character. In order to characterize these electronic transitions, rR spectra were recorded by excitation into these bands (Fig. 3, Table 1).

The merit of the rR technique is based on the fact that only those vibrations show a high Raman intensity that are coupled to the allowed electronic transition in which excitation takes place [36]. For comparison, the Raman spectrum of the free ligand was recorded under the same conditions. The resonance enhanced vibrations for both **1** and **2** can all be assigned to dmb ligand vibrations, although the intensities of the resonance Raman bands of the complexes differ from those of the free ligand. This difference is due to the fact that in resonance Raman the intensity of a particular band is mainly determined by the distortion of the compound in the excited state along the normal coordinate of that vibration, whereas the change in polarizability determines the intensity of an off-resonance Raman band. The observation of resonance enhanced dmb vibrations implies the involvement of this ligand in the electronic transition. The CO stretching frequency is not resonance enhanced, which implies that the charge density on the central metal atom is not affected by this transition, hence ruling out an MLCT assignment. This is supported by the observation that although, going from **1** to **2**, the electron density on the central metal atom increases (ν(CO) decreases), the absorption maximum remains unaffected. No alkyl ligand vibrations are resonance enhanced which makes it unlikely that the transition has SBLCT character, again agreeing with the R-group independence of the absorption maximum. Taking this into account, the lowest-energy absorption band most probably belongs to a halide-to-ligand charge transfer (XLCT) (X = I) transition, which is not unexpected in view of the presence of high lying filled p_π orbitals on I^-. A similar character of the lowest-energy electronic transition was found for [Re(I)(CO)$_3$(α-diimine)] [37], [Ru(I)(Me)(CO)$_2$(α-diimine)] [34], and [Pt(I)(Me)$_3$(^{i}Pr–DAB)] [7].

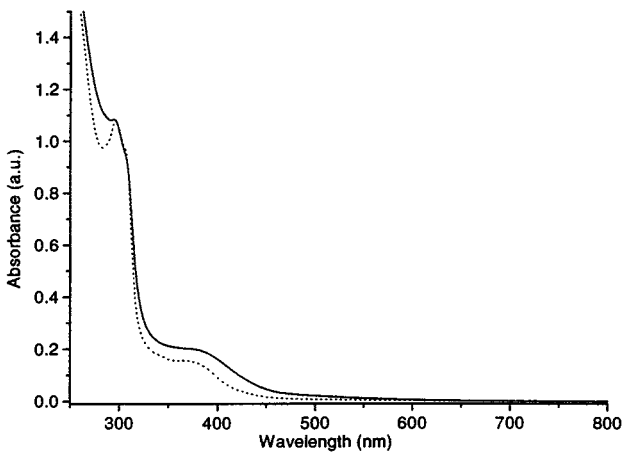

Fig. 2. Absorption spectra of **1** (dotted) and **2** (drawn) in THF.

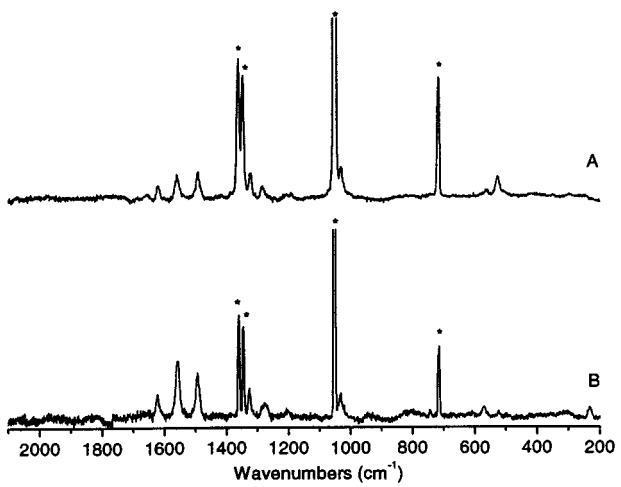

Fig. 3. Resonance Raman spectra of (A) **1** ($\lambda_{exc} = 457.9$ nm) at room temperature and (B) **2** ($\lambda_{exc} = 457.9$ nm) at 90 K in KNO_3. Asterisks denote nitrate bands.

3.4. Photochemistry

At room temperature, complex **1** does not show any photoreaction on irradiation with $\lambda_{irr} > 435$ nm, and the estimated quantum yield for **2** is less than 0.01 under these circumstances. Furthermore, the efficiency of the latter reaction strongly decreases on lowering the temperature and at -20°C, complex **2** is also virtually photostable. In order to study the primary photochemical step, a THF solution of **2** containing an excess of the spin-trap nitrosodurene, was irradiated in situ in an EPR spectrometer using a mercury lamp and a $\lambda_{irr} >$ 435 nm cutoff filter. Fig. 4 presents the EPR spectrum obtained on irradiation, as well as the PEST Winsim [38] simulated spectrum.

The complicated spectrum indicates that both the metal fragment radical and the alkyl radical are trapped by nitrosodurene. The best fit is obtained by assuming the presence of a small amount of a third EPR active species (probably free nitrosodurene radical), in addition to the nitrosodurene (nd) trapped isopropyl and metal fragment radicals. The hyperfine splitting constants for nd–^{i}Pr$^\bullet$ derived from the fitting procedure are $a_N = 13.59$ G and $a_H = 6.80$ G, in agreement with literature values of 13.8 and 6.7 G, respectively [39]. The fitted hyperfine constants for the nd trapped metal fragment are $a_N = 16.66$ G (nd), $a_{Rh} = 1.19$ G and $a_N = 2.16$ G (dmb). Due to the large linewidth of the latter radical (5.8 G) these last two values are not very reliable. The fact that they are small indicates that the

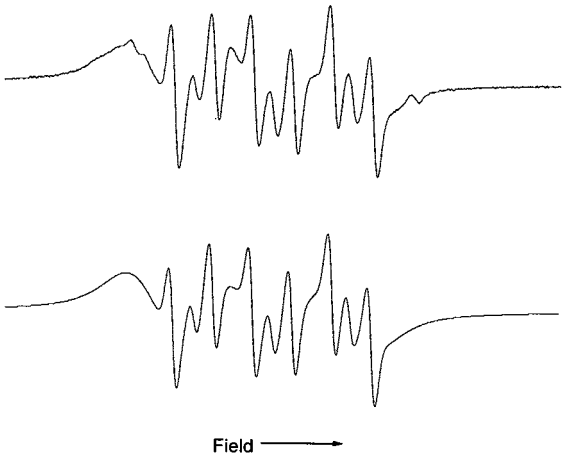

Fig. 4. Experimental (top) and simulated (bottom) EPR spectra obtained on irradiation ($\lambda_{irr} > 435$) of **2** in a THF solution containing an excess of nitrosodurene.

electron spin is mainly located on the nd nitrogen atom. Irradiation in the presence of an excess of PPh_3, previously used successfully to trap metal fragments selectively [40], did not result in any observable EPR signal. Attempted trapping experiments with ^{t}Bu-NO and PBN (phenyl-*N*-^{t}Bu-nitrone) proved also unsuccessful. The ^{t}Bu-NO has a dimeric structure and is itself more photoreactive than the complexes under investigation, which led to EPR spectra that were dominated by ^{t}BuNO$^\bullet$ signals. PBN, on the other hand, suffers from the disadvantage that the nearest proton of a trapped alkyl is in the γ position with respect to the unpaired electron of the spin trap, while the latter possesses a proton in the β position [41]. Indeed, in the EPR spectra obtained using this spin trap no hyperfine structure due to the trapped radical was observable.

As mentioned before, complex **1** is not photoreactive under these circumstances, and indeed no EPR spectrum was observed. However, irradiation at shorter wavelength ($\lambda_{irr} > 335$ nm) gives rise to the appearance of EPR signals, which are, however, not readily interpreted.

In order to identify photoproducts, THF solutions of **2** were irradiated in situ in IR and UV–vis spectrometers, using the 457.9 nm line of a Spectra Physics SP2025 Ar^+ laser. Similar irradiation times were needed for these experiments as for the EPR investigations, which indicates that bond homolysis is indeed the only photoprocess taking place for **2**. Upon irradiation ($P = 100$ mW) of **2** in THF, the ν(CO) band of the starting compound (2021 cm^{-1}) gradually disappears, while a new ν(CO) band appears at 2052 cm^{-1}. The photoproduct has less π backbonding to CO than the starting compound **2**, in view of the higher frequency of its ν(CO) band. Combined with the observation that the EPR spectra do not show the formation of a persistent radical in the absence of a spin-trap, it is proposed that this photoproduct is the [Rh(^{i}Pr)(I)(THF)(CO)(dmb)]$^+$ cation. This cation is the product of an electron transfer reaction of the [Rh(^{i}Pr)(I)(THF)(CO)(dmb)]$^\bullet$ radical that is formed by the homolysis of a Rh–^{i}Pr bond. Further support for this conclusion is gained from the fact that during the synthesis of **2**, an intermediate product is observed with a ν(CO) band at 2057 cm^{-1}, presumably belonging to a similar mono-alkylated species.

The UV–vis spectra are less informative. Irradiation of **2** in THF (457.9 nm, 100 mW) results in the disappearance of the absorption bands of the starting complex and the appearance of a new absorption band at ca. 360 nm. Upon prolonged irradiation aditionally an absorption band was observed at 425 nm. It appears that while the primary photochemical reaction is undoubtedly metal–alkyl bond homolysis, the subsequent chemical reactions are rather unselective, as has been observed previously for the isoelectronic [Pt(Me)$_4$(α-diimine)] complexes [42].

Although it was shown that the lowest energy allowed electronic transition has XLCT character, occupation of an XLCT excited state generally does not result in photochemical bond homolysis. Hence, the observed photoreaction must occur after crossing from the optically occupied XLCT state to a reactive one. Of the excited states known to give rise to bond homolysis, the SBLCT state is the most likely candidate. In such an SBLCT excited state electron density has been transferred from a bonding σ orbital to an empty ligand orbital. In the case of the complexes under study this corresponds to σ(Rh–R) $\rightarrow \pi^*$(dmb) charge transfer. Similar XLCT to SBLCT crossings were found for [Ru(I)(R)(CO)$_2$(^{i}Pr–DAB)] (R = ^{i}Pr, Bz) [15,16]. In general, the energy of the transition metal to carbon bond of a metal–alkyl complex increases with increasing σ donor strength of the alkyl group, decreasing the energy of the SBLCT-state. In the complexes under study, the ^{i}Pr group is the stronger σ donor. This explains that radical formation occurs at lower-energy irradiation for **2** than in the case of **1**.

4. Supplementary material

Crystallographic data for the structural analysis have been deposited with the Cambridge Crystallographic Data Centre, CCDC no. 150426. Copies of this information may be obtained free of charge from the Director, CCDC, 12 Union Road, Cambridge, CB2 1EZ, UK (fax: +44-1223-336033; e-mail: deposit@ccdc.cam.ac.uk or http://www.ccdc.cam.ac.uk).

Acknowledgements

This work was supported in part (M.L. and A.L.S.) by the Council for Chemical Sciences of the Netherlands Organization for Scientific Research (CW-NWO). B.C. de Pater is kindly thanked for his assistance with the syntheses.

References

[1] D.L. Morse, M.S. Wrighton, J. Am. Chem. Soc. 98 (1976) 3931.
[2] J.C. Luong, R.A. Faltynek, M.S. Wrighton, J. Am. Chem. Soc. 102 (1980) 7892.
[3] D.J. Stufkens, Comments Inorg. Chem. 13 (1992) 359.
[4] B.D. Rossenaar, C.J. Kleverlaan, M.C.E. van de Ven, D.J. Stufkens, A. Vlček Jr., Chem. Eur. J. 2 (1996) 228.
[5] B.D. Rossenaar, E. Lindsay, D.J. Stufkens, A. Vlček Jr., Inorg. Chim. Acta 250 (1996) 5.
[6] M.P. Aarnts, D.J. Stufkens, M.P. Wilms, E.J. Baerends, A. Vlček Jr., I.P. Clark, M.W. George, J.J. Turner, Chem. Eur. J. 2 (1996) 1556.
[7] J. van Slageren, S. Záliš, A. Klein, D.J. Stufkens, Inorg. Chem. (submitted).
[8] J. van Slageren, D.J. Stufkens, Inorg. Chem. 40 (2001) 227.
[9] J.J. Shiang, L.A. WalkerII, N.A. Anderson, A.G. Cole, R.J. Sension, J. Phys. Chem. B 103 (1999) 10532.
[10] H. Kunkely, A. Vogler, J. Organomet. Chem. 453 (1993) 269.
[11] P.I. Djurovich, R.J. Watts, Inorg. Chem. 32 (1993) 4681.
[12] P.I. Djurovich, R.J. Watts, J. Phys. Chem. 98 (1994) 396.
[13] P. Bradley, G. Suardi, A.P. Zipp, R. Eisenberg, J. Am. Chem. Soc. 116 (1994) 2859.
[14] C.J. Kleverlaan, D.J. Stufkens, I.P. Clark, M.W. George, J.J. Turner, D.M. Martino, H. van Willigen, A. Vlček Jr., J. Am. Chem. Soc. 120 (1998) 10871.
[15] C.J. Kleverlaan, D.J. Stufkens, J. Photochem. Photobiol. A: Chem. 116 (1998) 109.
[16] H.A. Nieuwenhuis, M.C.E. van de Ven, D.J. Stufkens, A. Oskam, K. Goubitz, Organometallics 14 (1995) 780.
[17] J.A. McCleverty, G. Wilkinson, Inorg. Synth. 8 (1966) 211.
[18] S. Hasenzahl, H.-D. Hausen, W. Kaim, Chem. Eur. J. 1 (1995) 95.
[19] A.L. Spek, PLATON, A Multipurpose Crystallographic Tool, Utrecht University, Netherlands, 1999.
[20] A. Altomare, M.C. Burla, M. Camalli, G.L. Cascarano, C. Giacovazzo, A. Guagliardi, A.G.G. Moliterni, G. Polidori, R. Spagna, J. Appl. Crystallogr. 32 (1999) 115.
[21] G.M. Sheldrick, SHELXL-97, Program for Crystal Sructure Refinement, University of Göttingen, Germany, 1997.
[22] M.A. Mitryaikina, L.S. Gracheva, V.K. Polovnyak, A.E. Usachev, Y.V. Yablokov, J. Gen. Chem. USSR 62 (1992) 821.
[23] P. Imhoff, R. van Asselt, C.J. Elsevier, M.C. Zoutberg, C.H. Stam, Inorg. Chim. Acta 184 (1991) 73.
[24] E. Delgado-Laita, E. Sanchez-Muñoyerro, Polyhedron 3 (1984) 799.
[25] R.D. Gillard, K. Harrison, I.H. Mather, J. Chem. Soc. Dalton Trans. (1975) 133.
[26] H. Van der Poel, G. van Koten, K. Vrieze, Inorg. Chim. Acta 51 (1981) 241.
[27] S. Morton, J.F. Nixon, J. Organomet. Chem. 282 (1985) 123.
[28] G. Mestroni, A. Camus, G. Zassinovich, J. Organomet. Chem. 65 (1974) 119.
[29] N.B. Pahor, R. Dreos-Garlatti, S. Geremia, L. Randaccio, G. Tauzher, E. Zangrando, Inorg. Chem. 29 (1990) 3437.
[30] S.-T. Mak, V.W.-W. Yam, C.-M. Che, T.C.W. Mak, J. Chem. Soc. Dalton Trans. (1990) 2555.
[31] D. Steinborn, M. Ludwig, J. Organomet. Chem. 463 (1993) 65.
[32] J.P. Collman, J.I. Brauman, A.M. Madonik, Organometallics 5 (1986) 310.
[33] R.C. Gash, D.J. Cole-Hamilton, R. Whyman, J.C. Barnes, M.C. Simpson, J. Chem. Soc. Dalton Trans. (1994) 1963.
[34] C.J. Kleverlaan, D.J. Stufkens, J. Fraanje, K. Goubitz, Eur. J. Inorg. Chem. (1998) 1243.
[35] P.K. Byers, A.J. Canty, B.W. Skelton, A.H. White, Organometallics 9 (1990) 826.
[36] R.J.H. Clark, T.J. Dines, Angew. Chem. Int. Ed. Engl. 25 (1986) 131.
[37] B.D. Rossenaar, D.J. Stufkens, A. Vlček Jr., Inorg. Chem. 35 (1996) 2902.
[38] D.R. Duling, J. Magn. Res. Ser. B 104 (1994) 105.
[39] C.J. Kleverlaan, D.J. Stufkens, Inorg. Chim. Acta 284 (1999) 61.
[40] M.P. Aarnts, D.J. Stufkens, A. Vlček Jr., Inorg. Chim. Acta 266 (1997) 37.
[41] E.G. Janzen, U.M. Oehler, D.L. Haire, Y. Kotake, J. Am. Chem. Soc. 108 (1986) 6858.
[42] W. Kaim, A. Klein, S. Hasenzahl, H. Stoll, S. Záliš, J. Fiedler, Organometallics 17 (1998) 237.